Vacancies and carbon impurities in α-iron: Electron irradiation

A. Vehanen, P. Hautojärvi, J. Johansson, and J. Yli-Kauppila
Laboratory of Physics, Helsinki University of Technology, SF-02150 Espoo 15, Finland

P. Moser
Section de Physique du Solide, Département de Recherche Fondamentale, Centre d'Etudes Nucléaires de Grenoble, 85 X, 38041 Grenoble Cédex, France
(Received 1 June 1981)

Positron-lifetime measurements are reported on electron-irradiated high-purity α-iron and on iron doped with controlled amounts of carbon impurities. We show that in pure iron monovacancies are mobile at stage III around 220 K causing vacancy clustering into small three-dimensional agglomerates. These clusters anneal out between 500 and 600 K. In carbon-doped iron a competing mechanism is the formation of a highly asymmetric carbon-vacancy pair at 220 K. These pairs dissociate around 490 K, resulting in another release of free vacancies in the lattice. Controversial aspects on vacancy properties in earlier investigations are discussed.

I. INTRODUCTION

Considerable efforts have been undertaken to clarify the behavior of point defects in α-iron. In spite of this, a consensus has not been reached on the elementary properties of vacancies and self-interstitial atoms. The reasons are in the difficulties on preparing high-purity specimens and in the high sensitivity of point defects to interstitial impurities. The situation has been reviewed by several authors.[1–4] Controversial results have been obtained concerning the position of the vacancy migration stage,[4–7] the suggested temperature regions extending from 200 to 550 K. On the other hand, the view of interstitial atom migration around 120 K has been generally accepted.[8]

Up to recent times, a considerable group of experiments including transmission electron microscopy,[9] magnetic relaxation,[10] studies of the onset for void swelling,[11] irradiation doping,[12] quenching,[13] internal friction,[14] as well as combined self-diffusion and positron annihilation measurements in thermal equilibrium,[15] seemed to point strongly towards a vacancy migration stage clearly above room temperature, at around 520 K. Yet a careful analysis of annealing kinetics by, e.g., Decker *et al.*[6] showed that the recovery stage around 220 K has to be assigned to the free migration of an elementary intrinsic point defect. Following the nomenclature in fcc metals, this stage was called the stage III of α-iron.[6] Although stage III in fcc metals is widely accepted to be due to monovacancy migration, Decker *et al.*[6] attributed this recovery stage to the migration of a second kind of interstitial atoms.

Carbon impurities have been observed to interact strongly with both interstitials[16] and with vacancy-type defects[17–19] in α-iron. This fact greatly influences the precipitation kinetics of carbon atoms[17–19] and has profoundly contributed to the difficulties in the interpretation of annealing stages. Free carbon-atom migration is known to occur at temperatures around 350 K.[7] The controversy on vacancy migration mentioned above brings up the question whether a mobile carbon interstitial is trapped by a stable monovacancy, or vice versa.

In this paper we follow the behavior of point defects in α-iron with positron-lifetime measurements. The method is highly defect specific,[20,21] since positrons tend to become trapped at vacancy-type defects, whereas they are completely insensitive to interstitial atoms and their small agglomerates. Furthermore, clustering of vacancies into small three-dimensional agglomerates is unambiguously detected. The positron lifetime increases rapidly when the cluster size grows from a monovacancy to a microvoid containing around 100 vacancies.[22] During further growth the lifetime saturates to a value of 500 psec as a large defect represents an internal surface of the metal.

We have performed positron-lifetime and residual-resistivity measurements in high-purity zone-refined α-iron as well as in iron doped with

carbon impurities. The present paper is the first of two papers. Here the specimens were damaged by electron irradiations at 20 K and by deformation at 77 K. The second part deals with fast neutron irradiations at 77 K. Our results presented in this paper show that free monovacancy migration indeed occurs at stage III around 220 K, resulting in formation of small vacancy agglomerates. Furthermore, the carbon atoms are observed to act as strong trapping sites for migrating monovacancies. Carbon-vacancy pairs formed at 220 K have a highly asymmetric character. Free carbon atoms migrating at 350 K interact further with vacancy complexes. The dissociation of carbon-vacancy pairs and vacancy agglomerates occurs around 490 and 550 K, respectively. In the second paper we show that in neutron-irradiated specimens, vacancy migration is shifted to 180 K due to the high local vacancy concentration within the collision cascades of the fast neutrons. Short communications on part of the work reported in these two papers have been published earlier.[23–26]

Section II of the present paper contains the experimental details. In Sec. III we consider the analysis of positron-lifetime spectra and relate the observable parameters with defect concentrations. Section IV describes the results of measurements in the electron-irradiated and deformed iron-carbon system. In Sec. V we present the positron-lifetime results in terms of concentrations of different vacancy-type defects. Section VI contains a discussion with some remarks on the contradictory results on vacancy properties in earlier investigations. Section VII includes the conclusion of the present work.

II. EXPERIMENTAL

The high-purity α-iron was prepared in Grenoble by zone-refining the Koch-Light starting material for one month in a helium atmosphere.[27] The ingot was then cold-rolled and specimens for positron and resistivity measurements were cut. These were annealed in a hydrogen atmosphere at 800 °C for 18 h. The residual resistivity ratio, measured in a longitudinal magnetic field of 50 mT, was $\Gamma=\rho(399\text{ K})/\rho(4.2\text{ K})=1500$. The carbon and nitrogen concentrations were estimated with the internal friction method. Total amount of these impurities was found to be less than 5 at. ppm.

Carbon doping was performed by melting the iron with pure graphite in an induction furnace under a helium atmosphere. After cold-rolling and cutting, a solution-annealing treatment was given to the samples in a helium atmosphere at 750 °C. The specimens were then quenched into icy water, electrolytically polished, and stored at liquid nitrogen temperature. Two sets of samples were made with the carbon concentrations of 50 and 750 at. ppm. The first value was obtained from a chemical analysis while the second value was estimated from the amounts of iron and graphite placed in the induction furnace. The sample dimensions were $6\times8\times0.3$ mm^3 for positron experiments and $\phi=0.6\times100$ mm^3 for residual resistivity measurements.

Electron irradiations were carried out in Grenoble under liquid hydrogen by using a 3-MeV Van de Graaff accelerator with beam currents 10–20 μA. The samples were transported to Helsinki at 77 K for positron measurements. Plastic deformation was performed by pressing the specimens slowly in a liquid-nitrogen bath. The thickness reduction was about 60%. After deformation the samples were directly transferred into a cryostat for positron measurements at 77 K.

Some data on the studied samples are collected in Table I. For each specimen we give the method of defect production, irradiation-induced resistivity increase (measured after 77 K anneal), irradiation dose, carbon concentration, the positron emitter used in the measurements, and the resolution of the positron-lifetime equipment.

Positron-lifetime spectra were measured with a conventional fast-slow coincidence device[20] having the time resolution shown in Table I. A positron source was sandwiched between two identical samples under liquid nitrogen. As a positron emitter we used a normal ^{22}Na source made by evaporating about 10 μCi of aqueous ^{22}NaCl solution onto a thin (1.14 mg/cm^2) nickel foil. We also prepared a ^{48}V source[28] of about 15 μCi by irradiating a thin (0.8 mg/cm^2) titanium foil with 20-MeV protons at the Cyclotron Laboratory of the University of Jyväskylä, Finland. This source allowed measurements of lifetime spectra with an order-of-magnitude smaller long-lifetime source correction.[28,29] During a typical 15-ksec measuring time 6×10^5 lifetime events were collected.

During the isochronal annealing treatments the samples were heat treated for 30 min in 20 K temperature intervals. A temperature-stabilized (±1 K) furnace with a pure helium atmosphere was used except for the heat treatments for pure iron above 340 K, which were carried out in a purified hydrogen atmosphere. Positron measure-

TABLE I. Sample data. Electron irradiations were made at 20 K and deformation at 77 K. The irradiation-induced resistivity increase is given after 77-K annealing.

Sample	Defect production	$\Delta\rho_{irr}$ (nΩ cm)	Dose or thickness reduction	Carbon concentration (at. pmm)	Positron source	Resolution of lifetime system (FWHM, psec)
A	e^- irr	140	3×10^{18} e^-/cm^2	<5	^{22}Na	290
B	e^- irr	310	6×10^{18} e^-/cm^2	<5	^{22}Na	290
C	e^- irr	1600[a]	3×10^{19} e^-/cm^2	50	^{22}Na	290
D	e^- irr	1600[a]	3×10^{19} e^-/cm^2	750	^{22}Na	290
E	e^- irr	150[a]	3×10^{18} e^-/cm^2	50	^{22}Na	250
F	e^- irr	50[a]	1×10^{18} e^-/cm^2	50	^{48}V	225
G	def.		60%	<5	^{22}Na	290

[a]Estimated from the irradiation dose.

ments were performed in vacuum at 77 K, except for the samples *A* to *D* (Table I), which were measured at room temperature after 340-K annealing. The increase in the measuring temperature was simply due to an increased data accumulation rate obtained with a more effective sample-detector geometry.

III. ANALYSIS OF POSITRON EXPERIMENTS

A thermalized positron in a perfect metal shows a constant annihilation rate λ_f. Thus the lifetime distribution measured in an annealed α-iron consists of a single exponential component and the number of positrons in the lattice left at time t after their emissions is

$$n_f(t)=n_0\exp(-\lambda_f t)=n_0\exp(-t/\tau_f)\ , \qquad (1)$$

where n_0 is the total number of observed annihilation events. $\tau_f=1/\lambda_f$ is the positron lifetime. For iron we have $\tau_f=110$ psec. In the presence of vacancy-type defects, positrons tend to get localized at their sites. This results in a lifetime distribution consisting of a sum of several exponential components. The number of positrons in the lattice containing N different types of vacancy defects now becomes

$$n_d(t)=n_0\sum_{i=1}^{N+1} I_i\exp(-t/\tau_i)\ . \qquad (2)$$

Here I_i denotes the relative intensity of the component having the lifetime value τ_i ($\sum_{i=1}^{N+1} I_i=1$). The lifetimes τ_i of trapped positrons are considerably longer than τ_f due to a lower electron density within the defects. The average positron lifetime or the statistical mean of the positron-lifetime distribution is defined by

$$\bar{\tau}=\sum_{i=1}^{N+1} I_i\tau_i\ . \qquad (3)$$

In the following we relate the observable parameters τ_i and I_i with the properties of defects present in the lattice. We assume that no detrapping of positrons occurs from the localized states.

A. Positron trapping in the presence of a single type of defect ($N=1$)

Assume a concentration c_v of defects which we take here to be monovacancies. The positron trapping probability is directly proportional to the de-

fect concentration. Denoting the specific trapping rate as μ_v, the positron trapping rate κ_v becomes

$$\kappa_v = \mu_v c_v \ . \tag{4}$$

According to Eq. (2), the observed lifetime distribution is a superposition of two exponential components with the values of the observable parameters[30]:

$$\tau_1 = \frac{\tau_f}{1+\kappa_v \tau_f} \ , \tag{5a}$$

$$\tau_2 = \tau_v = \lambda_v^{-1} \ , \tag{5b}$$

and

$$I_2 = \frac{\kappa_v}{\lambda_f - \lambda_v + \kappa_v} \ , \tag{5c}$$

from which we get

$$\kappa_v = \frac{I_2}{I_1}(\lambda_f - \lambda_v) \ . \tag{5d}$$

Above, $\tau_v = \lambda_v^{-1}$ represents the trapped positron lifetime in a monovacancy. For iron $\tau_v = 175$ psec (see Sec. IV). The specific trapping rate for monovacancies in iron is estimated in Sec. V to be $\mu_v = (1.1 \pm 0.2) \times 10^{15}$ sec^{-1}, which is in good agreement with the result of Schäfer *et al.*[31] Equations (4) and (5d) directly give the defect concentration in the lattice, while Eq. (5a) can be used for checking the internal consistency in the analysis. In the limits of very low ($\kappa_v << \lambda_f$) or very high ($\kappa_v >> \lambda_f$) defect concentrations, the measured lifetime spectrum becomes one-exponential with $\tau = \tau_f$ or $\tau = \tau_v$, respectively.

B. Positron trapping in the presence of two types of defects ($N = 2$)

The lattice contains two different positron traps with concentrations c_v and $c_{\rm cl}$. The corresponding specific trapping rates are μ_v and $\mu_{\rm cl}$, respectively. Here the nomenclature c_v (vacancy-type defects) and $c_{\rm cl}$ (vacancy clusters) serves for further needs. The trapped positron lifetimes are τ_v and $\tau_{\rm cl}$. The measured lifetime distribution is now three-exponential with[30]

$$\tau_{\rm I} = \frac{\tau_f}{1+\kappa_v \tau_f + \kappa_{\rm cl} \tau_f} \ , \tag{6a}$$

$$\tau_{\rm II} = \tau_v = \lambda_v^{-1} \ , \tag{6b}$$

$$\tau_{\rm III} = \tau_{\rm cl} = \lambda_{\rm cl}^{-1} \ , \tag{6c}$$

$$I_{\rm I} = 1 - I_{\rm II} - I_{\rm II} \ , \tag{6d}$$

$$I_{\rm II} = \frac{\kappa_v}{\lambda_f - \lambda_v + \kappa_v + \kappa_{\rm cl}} \ , \tag{6e}$$

and

$$I_{\rm III} = \frac{\kappa_{\rm cl}}{\lambda_f - \lambda_{\rm cl} + \kappa_v + \kappa_{\rm cl}} \ . \tag{6f}$$

In the above equations $\kappa_{\rm cl} = \mu_{\rm cl} c_{\rm cl}$. In principle, by applying a three-component fit one can resolve the interesting parameters $\kappa_{\rm cl}$ and κ_v. However, this cannot be realized in practice, since an unrestricted three-component decomposition results in an unacceptable amount of scatter in the analyzed lifetimes τ_i and intensities I_i.

C. Practical considerations

In addition to annihilation events from the sample the measured lifetime spectra contain annihilation events from the positron source material too. After subtracting the source contribution and a random background we decompose the resulting multiexponential lifetime spectrum into the intensities I_i and lifetimes τ_i in Eq. (2). These parameters should then be connected to the defect concentrations present in the lattice. However, the values of the parameters often contain considerable scatter and care must be taken before the results from a lifetime spectrum analysis are interpreted in terms of physical properties of defects.

A feature deserving special attention is that the average positron lifetime $\bar{\tau}$ is a statistically more reliable parameter to describe the measured distribution than the individual components obtained from the decomposition. The average lifetime can be calculated in two ways, either from the experimental data points as the first moment of the spectrum about the time zero or from the analyzed lifetimes τ_i and their relative intensities I_i by applying Eq. (3). When fitting the spectra we have required that these two methods give the same value of $\bar{\tau}$ within 2 psec. If not, it indicates that the lifetime distribution is distorted by, e.g., exceptional experimental drifts or that an improper resolution function has been used. Sometimes the decomposition may be difficult and it may result in unreasonable values for the parameters although a satisfactory variance is obtained. However, in case the fitted curve matches well the data points in all parts of the spectrum, the first moment of the fitted curve equals the first moment of the ex-

perimental lifetime distribution, and consequently the average lifetime determined from Eq. (3) is correct. In the following we make use of this feature.

In the presence of defects of single type we analyze the spectrum with two components to obtain a value for the average positron lifetime $\bar{\tau}$. In case the trapped positron lifetime is known (e.g., $\tau_v = 175$ psec for monovacancies in iron), we combine Eqs. (3) and (5) and get the trapping rate

$$\kappa_v = \lambda_f \frac{\bar{\tau} - \tau_f}{\tau_v - \bar{\tau}} . \tag{7}$$

Because of the good statistical properties of $\bar{\tau}$, more accurate values for κ_v are expected when this formula is used instead of Eq. (5d).

When there are two types of defects in the lattice (vacancies and vacancy clusters) we can, in principle, apply a three-component fit and resolve the parameters κ_{cl} and κ_v from Eqs. (6) to estimate the concentrations of the two defects. However, in practice the statistical uncertainties of the analyzed lifetimes and intensities are too large because of the high number of free variables. Therefore, we decompose the spectra using only two lifetime components with fitting parameters τ_1, τ_2, and I_2. In all cases this was also found to result in a satisfactory variance. As the longest lifetime component (of the order of 300 psec or more) is clearly separated from other parts of the spectrum (see e.g., Fig. 1), we assume that the decomposition

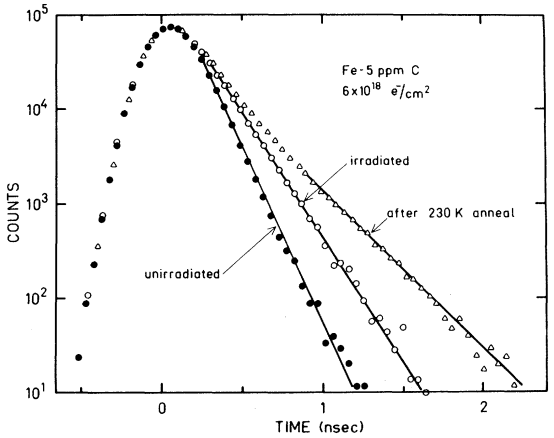

FIG. 1. Positron-lifetime spectra after source-background subtraction in electron-irradiated (6×10^{18} e^-/cm^2) high-purity iron at various stages of isochronal annealing. The dramatic occurrence of a long-lifetime component after 230 K annealing is clearly visible.

procedure results in the correct values for the longest lifetime component, i.e.,

$$\tau_2 = \tau_{III} \tag{8a}$$

and

$$I_2 = I_{III} . \tag{8b}$$

As discussed earlier the average positron lifetime is also obtained correctly in the case of a satisfactory fit, i.e.,

$$\begin{aligned}\bar{\tau} &= \tau_I I_I + \tau_{II} I_{II} + \tau_{III} I_{III} \\ &= \tau_1 I_1 + \tau_2 I_2 .\end{aligned} \tag{9}$$

A direct consequence is that τ_1 describes the mean lifetime for positrons annihilating with lifetimes τ_I and τ_{II}, i.e.,

$$\begin{aligned}\tau_1 &= \frac{\tau_I I_I + \tau_{II} I_{II}}{I_I + I_{II}} \\ &= \frac{1 + \tau_v \kappa_v [1 + \kappa_{cl}/(\lambda_f - \lambda_{cl} + \kappa_v)]}{\lambda_f + \kappa_v + \kappa_{cl}}\end{aligned} \tag{10a}$$

$$I_1 = I_I + I_{II} . \tag{10b}$$

The latter expression for τ_1 follows from Eqs. (6).

We can now solve the positron trapping rates κ_v and κ_{cl} and thus, if the specific trapping rates μ_v and μ_{cl} are known, also determine the defect concentrations c_v and c_{cl}. For the trapping rates we obtain from Eqs. (6), (8), and (10):

$$\kappa_v = \frac{\tau_1(\lambda_f - I_2\lambda_{cl}) - I_1}{\tau_v - \tau_1} \tag{11a}$$

and

$$\kappa_{cl} = \frac{I_2}{I_1}(\lambda_f - \lambda_{cl} + \kappa_v) . \tag{11b}$$

The trapping rates in the two cases discussed above are calculated in Sec. V. In case a distinct long-lifetime component is observed, we also check whether the analysis is compatible with one defect type only. From the values of τ_2 and I_2 we calculate the trapping rate κ_{cl} from Eq. (5c). This value is then used to evaluate τ_1 from Eq. (5a). These τ_1 values are indicated with dashed lines in the figures of Sec. V. If the experimental τ_1 values are higher, then according to Eq. (10a), τ_1 is due to annihilations of both free positrons and those trapped at additional defects present in the lattice. Hence our conclusion is that in this case at least two defect types must be present in the specimen to account for the results from the exponential decomposition.

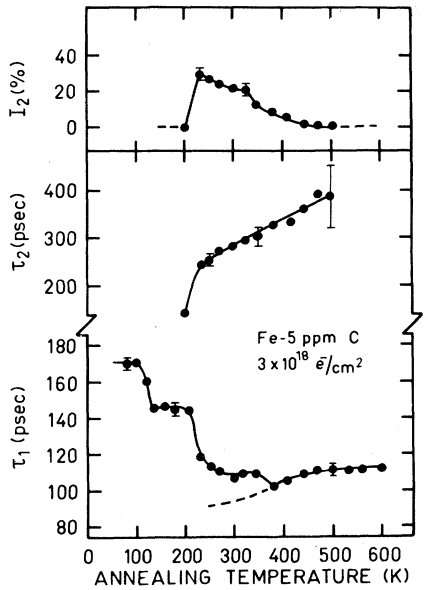

FIG. 2. Positron-lifetime parameters as a function of the isochronal annealing temperature in the low-dose electron-irradiated pure iron. The error bars are statistical standard deviations from the fit. The dashed line for τ_1 follows from trapping model assuming the presence of vacancy clusters only.

The specific trapping rates themselves depend on the temperature, where the positron-lifetime measurements are performed. It is generally agreed that the monovacancy trapping rate μ_v is temperature independent, while the trapping rate μ_{cl} into more extended defects increases with temperature.[32]

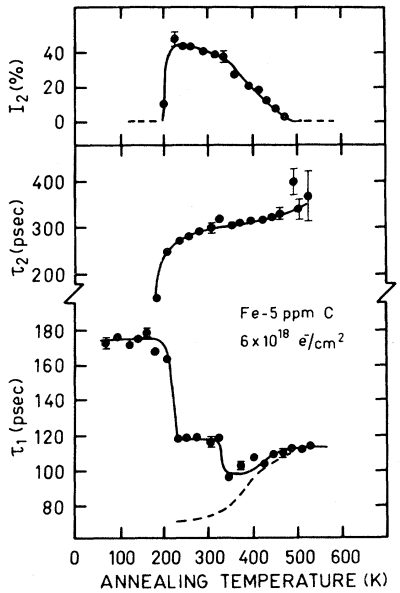

FIG. 3. Positron-lifetime parameters as a function of the isochronal annealing temperature in the high-dose electron-irradiated pure iron. For the dashed line in τ_1 see Fig. 2.

IV. RESULTS

A. Electron-irradiated pure iron

Two high-purity α-iron specimens (samples *A* and *B* in Table I) were electron-irradiated to doses 3×10^{18} and 6×10^{18} e^-/cm^2. Positron-lifetime spectra in these samples are observed to depend strongly on the annealing temperature. Some examples are shown in Fig. 1 for the high-dose irradiated specimen. The positron-lifetime parameters τ_1, τ_2, and I_2 as a function of the isochronal annealing temperature are shown in Figs. 2 and 3. The irradiation-induced resistivity increases (Table I) at 77 K correspond to Frenkel-pair concentrations of 47 and 103 ppm when the value of 30 μΩ cm/at. % for Frenkel-pair resistivity[8] is used.

After the low-dose electron irradiation the positron-lifetime spectrum is one-exponential between 77 and 100 K, with a mean lifetime $\bar{\tau}=175$ psec. This indicates that all positrons are trapped by defects, i.e., by monovacancies produced in electron irradiation (cf. Sec. III A), and consequently the lifetime is that of positrons at monovacancies, $\tau_v=175$ psec. During annealing through stage I_E at 120 K a decrease in τ_1 is observed. This corresponds to a decrease in monovacancy concentration due to Frenkel-pair recombinations by migrating self-interstitial atoms. No further changes in the lifetime distribution are observed before annealing at 220 K, where a distinct long-lifetime component abruptly arises having the lifetime $\tau_2=300$ psec and the intensity $I_2\cong20\%$. At the same time τ_1 decreases strongly to a level of about 110 psec. In agreement with earlier observations in copper,[33,34] molybdenum,[35] and tungsten,[36] as well as with theoretical predictions[22] we attribute this long-lifetime component to positron trapping into three-dimensional vacancy clusters. Thus monovacancies produced in electron irradiation migrate freely during stage III and form small vacancy clusters. A contradictory explanation for the long-lifetime component has been presented[31,37] in terms of positron trapping at interstitial agglomerates. However, this idea has neither theoretical nor experimental basis.[22,38] Our results thus confirm the early suggestion of Cuddy[5] that free monovacancy migration occurs already at 220 K.

During further annealing above stage III we observe a continuous growth of vacancy clusters seen

as an increase in τ_2 in Fig. 2. These vacancy agglomerates anneal out finally around 500 K. When we consider the behavior of τ_1 after stage III we observe that between 220 and 350 K the level of τ_1 is slightly above the dashed line, which shows the value of τ_1 in case we take into account positron trapping into vacancy clusters only. The difference is, however, too small for any detailed discussion.

The annealing behavior of pure iron irradiated to the higher dose (sample *B* in Table I) is indicated in Fig. 3. The gross features of Fig. 2 are well reproduced with some important exceptions. Firstly, above 120 K, τ_1 still stays at the level of 175 psec corresponding to saturation trapping at monovacancies. This is due to the higher irradiation dose; after the stage I_E the vacancy concentration is still high enough to account for 100% trapping probability of positrons. After stage-III annealing we again observe a distinct long-lifetime component due to the formation of vacancy clusters. This is extremely visible from the broadening of the lifetime spectrum in Fig. 1. The increase of the size of vacancy clusters occurs gradually during further annealing. Vacancy clusters have annealed out totally as the annealing temperature of 500 K is reached.

The dashed line in Fig. 3 again shows the value of τ_1 obtained from Eq. (5a) when vacancy clusters are assumed to be the only positron traps existing in the lattice. We notice that the measured values of τ_1 between 200 and 400 K are clearly above this line. Thus the vacancy clusters alone cannot explain the results, but it seems that in addition to the clusters, a fraction (although quite small) of other vacancylike defects survive in the lattice beyond stage III. This might be due to vacancy capture by immobile impurities resulting in a complex still capable of trapping positrons. Another possibility might be formation of dislocation loops from vacancies during their migration.

The prominent features in the annealing of pure electron-irradiated iron are the following: (1) Migration of self-interstitials and recombination of a fraction of Frenkel pairs at 120 K. (2) Migration of monovacancies at 220 K resulting in the formation of small vacancy agglomerates. (3) Dissociation of vacancy clusters at 500 K.

B. Deformed pure iron

High-purity iron samples (specimen *G* in Table I) were deformed plastically by pressing under liquid nitrogen up to a thickness reduction of 60%. The positron-lifetime parameters as a function of isochronal annealing temperature are shown in Fig. 4. Below 200 K we notice that the lifetime spectrum is one-exponential with the average positron lifetime $\tau_1 = 165$ psec. This corresponds to 100% positron trapping at dislocations and vacancies produced during plastic deformation.[39] The lifetime value $\tau = 165$ psec is slightly lower than the monovacancy lifetime $\tau_v = 175$ psec. This behavior seems to be common for a variety of metals.

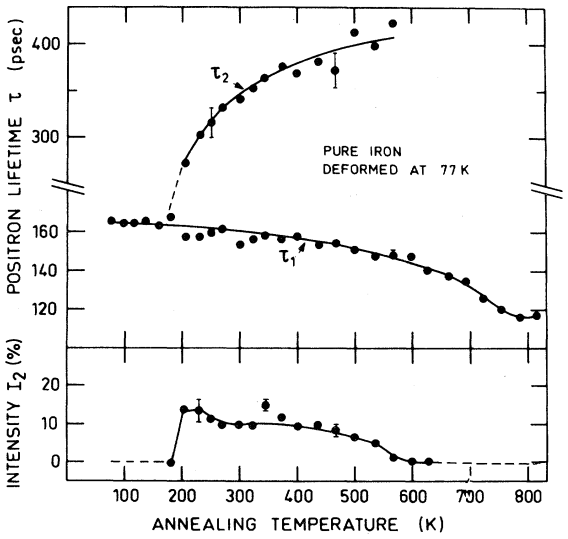

FIG. 4. Positron-lifetime parameters as a function of the isochronal annealing temperature in plastically deformed pure iron.

After annealing through stage III we again observe the appearance of a long-lifetime component with $\tau_2 \simeq 300$ psec and $I_2 \simeq 13\%$. Thus vacancies which are also produced during plastic deformation, become mobile and form small agglomerates or microvoids after 200 K annealing. At higher temperatures a continuous increase in the longer lifetime values τ_2 is observed, indicating a coarsening of the microvoid structure.

Above 500 K the intensity I_2 gradually drops to zero as the vacancy agglomerates become thermally unstable. After 600 K positrons are trapped at the remaining dislocations only. The decrease of τ_1 is very smooth, indicating the occurrence of a recrystallization process. Finally, after 800 K annealing the average positron lifetime reaches a value of 110 psec, characteristic for a defect-free lattice.

To sum up, our measurements on deformed pure iron demonstrate the formation of vacancy agglomerates at 220 K, showing again that the vacancy migration takes place at this temperature.

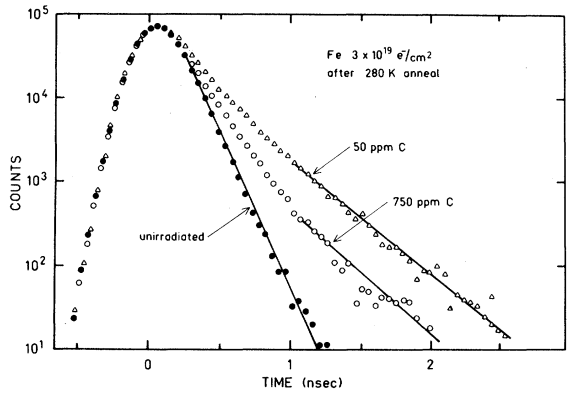

FIG. 5. Positron-lifetime spectra after source-background subtraction in electron-irradiated (3×10^{19} e^-/cm^2) Fe—50 at. ppm C and Fe—750 at. ppm C specimens after 280 K annealing. The effect of carbon on the width of the lifetime spectrum is clearly seen.

Thus the results are in good agreement with those in electron-irradiated iron presented in Sec. IV A.

C. Electron-irradiated carbon-doped iron

To investigate the effect of carbon atoms on the annealing behavior of point defects we electron-irradiated two pairs of specimens with carbon concentrations 50 and 750 at. ppm, respectively, to doses of 3×10^{19} e^-/cm^2 (samples *C* and *D* in Table I). Examples of the lifetime spectra are seen in Fig. 5. The positron-lifetime parameters as a function of the isochronal annealing temperature are shown in Figs. 6 and 7 for the two specimens. The measured lifetime spectra show again one-exponential behavior between 77 and 200 K with $\tau_1=\tau_v=175$ psec. Due to the very high irradiation dose, positrons detect only monovacancies in the lattice below stage III, and their concentration is high enough for saturation trapping.

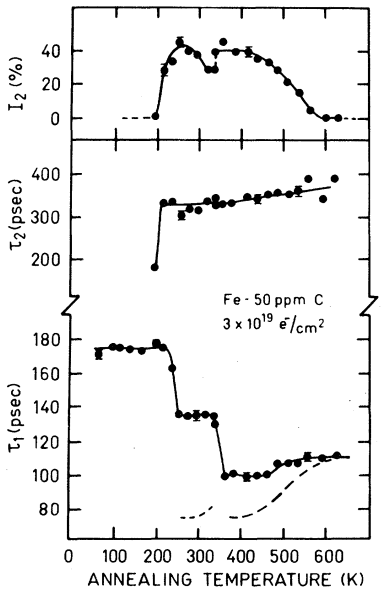

FIG. 6. Positron-lifetime parameters in the electron-irradiated Fe—50 at. ppm C sample after isochronal annealings. For the dashed line in τ_1 see Fig. 2. The vertical shift at 340 K is due to a change in the measuring temperature.

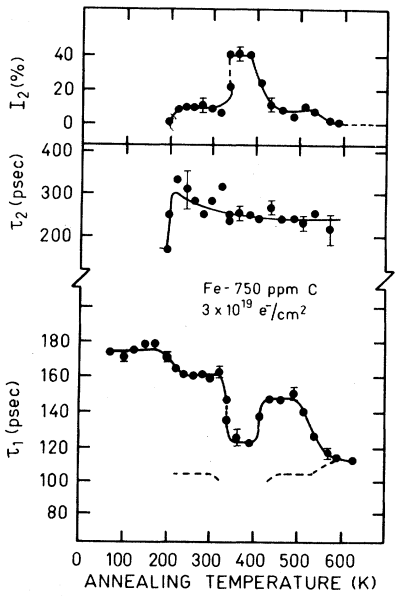

FIG. 7. Positron-lifetime parameters as a function of the isochronal annealing temperature in the electron-irradiated Fe—750 at. ppm C sample. For the dashed line in τ_1 see Fig. 2.

The annealing of the specimens through stage III causes a clear splitting of the lifetime curves into two exponential components, with the longer lifetime value $\tau_2\cong300$ psec. The corresponding intensities after stage III are $I_2\cong40\%$ and $I_2\cong10\%$ in the specimens containing 50 and 750 at. ppm C, respectively. The free migration of monovacancies during stage-III annealing is thus manifested by the formation of vacancy agglomerates also in carbon-doped iron specimens. Yet, by comparing Figs. 6 and 7, the tendency of vacancies to form clusters decreases with carbon additions. This is seen as a decrease in I_2 as the concentration of carbon impurities is increased. This is also very clearly noticed by comparing the two lifetime spectra in Fig. 5 measured after annealing above stage III.

The annealing behavior of the shorter lifetime component τ_1 in the carbon-doped specimens shown in Figs. 6 and 7 contains considerably more structure than in the case of pure iron in Figs. 2 and 3. Again the dashed lines in the figures show the values of τ_1 as calculated from Eq. (5a) when only positron trapping into vacancy clusters is taken into account. We observe that between 200 and 300 K the experimental data points for τ_1 are significantly above the dashed lines. This indicates that in addition to the clusters, some other positron traps exist in the lattice. The values of the shorter lifetime τ_1 from Figs. 3, 6, and 7 have been collected in Fig. 8. In all curves a strong decrease in τ_1 is seen at 200 K. Between 220 and 350 K the τ_1 values remain constant, but the height of the level increases strongly with the carbon concentration. This means that the more there are carbon impurities in the lattice, the more the vacancies survive the stage-III annealing. Thus monovacancies migrating at stage III interact strongly with carbon impurities. We ascribe this phenomenon to the capture of migrating vacancies by carbon atoms, which are known to be immobile at these temperatures. Vacancies trapped by carbon atoms retain their capability of attracting positrons; it is the presence of these "frozen" vacancies which gives rise to an increased level of τ_1 after 200 K anneal.

The estimated vacancy concentrations in the carbon-doped specimens just below 200 K are around 100 ppm (cf. Sec. V B), i.e., comparable to the carbon concentration in the Fe—50 at. ppm C specimen (sample *C*). In this sample the level of τ_1 is 135 psec, suggesting a considerable positron trapping into the carbon-vacancy pairs already at this concentration. In the sample containing 750 at. ppm C (sample *D*), the pair concentration is expected to be much higher and yet the change in the level of τ_1, from 135 to 160 psec is relatively small. Consequently, we take $\tau_1 = 160$ psec as the saturation value giving the trapped positron lifetime in the carbon-vacancy pair. We also notice that even in the nominally "pure" iron (< 5 at. ppm C) samples a faint indication of carbon-vacancy pairs is observed, as discussed in connection with Figs. 2 and 3.

The next annealing stage in Fig. 8 is observed at 350 K, where free migration of carbon interstitials occurs. In all cases τ_1 decreases strongly, indicating the loss of vacancy-type defects. We interpret this as further decoration of carbon-vacancy pairs with migrating carbon atoms, which leads to the disappearance of the positron trapping capability

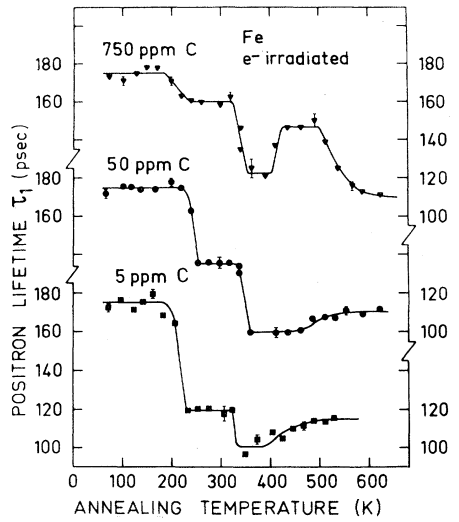

FIG. 8. Shorter positron-lifetime values τ_1 as a function of the isochronal annealing temperature from Figs. 3, 6, and 7.

of the decorated pairs.

The formation of carbon-vacancy pairs also has a clear effect on the behavior of τ_2 and I_2. As is seen from Figs. 6 and 7, the lifetime τ_2 is about the same in both carbon-doped specimens, but instead its intensity I_2 is much smaller in the case of the higher carbon concentration (see also Fig. 5). This is due to the increased capture of vacancies by carbon atoms, which results in a reduced number of vacancy clusters. Because of the very low carbon concentration, the intensity I_2 in pure iron (Fig. 3) reaches a value of 45%—the same as in Fig. 6—even though the irradiation dose is a factor of 5 smaller.

A discontinuity in the I_2 values is observed in Figs. 6 and 7 at 340 K. This is due to a change in the measuring temperature from 77 K to room temperature. The specific trapping rate μ_{cl} for vacancy clusters increases with the temperature, while that for monovacancies μ_v stays constant. The existing vacancy clusters thus become more effectively detected by positrons at the expense of carbon-vacancy pairs. The same discontinuity is also reflected as a decrease in τ_1. At the same temperature region, around 350 K, we also observe a decrease in τ_1 due to isochronal annealing treatments. As discussed previously, this is caused by the migration of carbon atoms which are captured by the carbon-vacancy pairs. The resulting monovacancy-polycarbon complex does not contain free space for positron trapping. Actually there exists a competition between positron trapping into

the vacancy clusters and into the carbon-vacancy pairs. Owing to the change in the measuring temperature and the passing of the carbon migration stage, positron trapping starts favoring the vacancy agglomerates. A reverse situation occurs at 400 K in the Fe—750 at. ppm C sample: the balance in the positron trapping process turns towards an increased trapping into the vacancy-type defects.

The stability of carbon-vacancy pairs is not revealed by our results shown in Figs. 6 and 7. This is due to the further decoration of the pairs caused by carbon migration at 350 K. In order to obtain information on the annealing behavior of carbon-vacancy pairs above 350 K, we irradiated two Fe—50 at. ppm C specimens to electron doses of 3×10^{18} and 1×10^{18} e^-/cm^2 (samples E and F in Table I). The idea of the smaller irradiation dose was to decrease the vacancy concentration with respect to carbon concentration below stage III and thus to favor carbon-vacancy pair formation at the expense of vacancy clustering. Further, we measured the positron lifetime in these samples at 77 K, also after annealing treatments above 340 K. Thus we could make use of the temperature-dependent positron trapping into vacancy clusters. At 77 K the existing carbon-vacancy pairs are detected more effectively by positrons because the specific trapping rate into vacancy clusters is lower than its value at room temperature, while the specific trapping rate into carbon-vacancy pairs remains constant.

The positron parameters as a function of the isochronal annealing temperature are shown in Figs. 9 and 10 for the specimens irradiated to the electron doses of 3×10^{18} and 1×10^{18} e^-/cm^2, respectively. Results for the latter case are shown only after 300 K annealing. In the sample irradiated to the higher dose the lifetime spectra below stage I_E contain only one component with a value $\tau=\tau_v=175$ psec, as seen in Fig. 9. This means that all positrons are trapped by vacancies. After 120 K annealing the lifetime drops to a value of 155 psec: the vacancy concentration diminishes to a level where only about 70% of positrons are trapped. An analogous behavior was found in the case of low-dose electron-irradiated pure iron (cf. Fig. 2). After stage-III annealing a long-lifetime component is again developed with $\tau_2\cong300$ psec, while $I_2\cong8\%$ is rather small due to a low irradiation dose and a high relative carbon concentration.

From Figs. 9 and 10 we observe that after stage III the level of τ_1—being 140 and 126 psec, respectively—is again much too high to account for positrons trapping into vacancy clusters only. Analogously with Fig. 8, we ascribe this behavior to positron trapping into carbon-vacancy pairs.

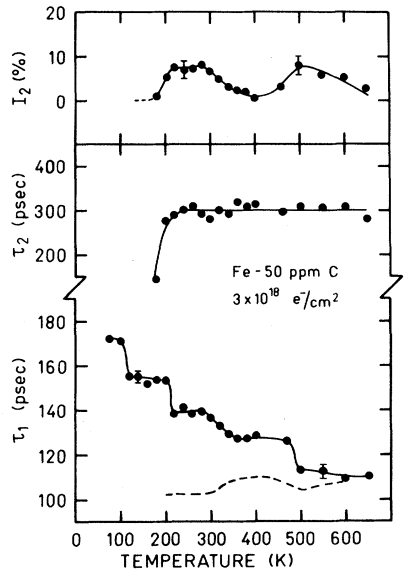

FIG. 9. Positron-lifetime parameters in the Fe-50 at. ppm C specimen after the lower-dose electron irradiation as a function of the isochronal annealing temperature. The dashed line for τ_1 follows from the trapping model assuming the presence of vacancy clusters only.

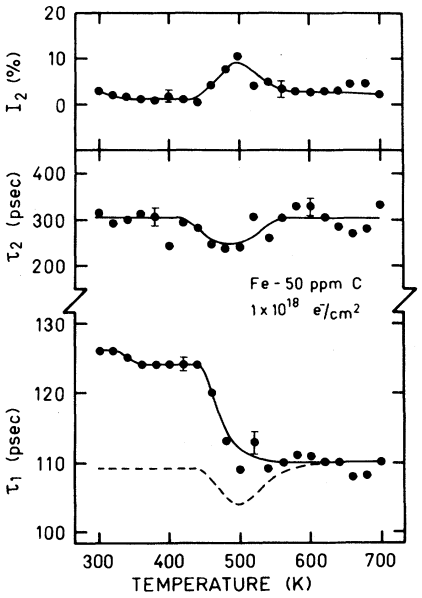

FIG. 10. Positron-lifetime parameters as a function of the isochronal annealing temperature in the Fe—50 at. ppm C specimen after the lowest-dose electron irradiation. For the dashed line in τ_1 see Fig. 9.

Owing to the higher irradiation dose in Fig. 9, the values of τ_1 and I_2 are higher compared to those in Fig. 10.

The carbon migration stage at 350 K causes relatively small changes in the positron parameters shown in Figs. 9 and 10. In both cases τ_1 decreases only slightly. In Fig. 9, I_2 drops to a very small level while in Fig. 10 it is small already before the carbon migration stage. Thus the free carbon atoms available after stage III make a part of both vacancy clusters and carbon-vacancy pairs ineffective to trap positrons by further decorating the existing defect complexes. Contrary to the case in Fig. 6, the level of τ_1 in Figs. 9 and 10 stays high also beyond 350 K. Positrons seem to detect vacancy-type defects also after the carbon migration. Thus some carbon-vacancy pairs are not decorated with additional carbon atoms. It may also be possible that some monovacancy-poly-carbon complexes contain a sufficiently small number of carbon atoms to maintain their capability as positron traps.

During further annealing above 350 K, the level of τ_1 stays constant in Figs. 9 and 10 until 490 K, where a sharp decrease is observed in both cases. This means that at 490 K the disappearance of carbon-vacancy complexes still capable of positron trapping occurs. At the same temperature range we notice a slight increase in I_2, i.e., positron trapping into vacancy clusters is enhanced. We ascribe this behavior to the dissociation of carbon-vacancy pairs or complexes. Thus we are again dealing with a recovery stage associated with a release of free monovacancies to the lattice. These vacancies form clusters, which cause increased positron trapping into vacancy agglomerates seen as an increase in I_2. Above 500 K, vacancy clusters remain the only kind of defects which are detected by positrons. During further annealing these agglomerates disappear at 700 K.

Our main results on electron-irradiated iron-carbon systems may be summarized as follows. (1) Vacancies are mobile at stage III around 220 K, resulting in formation of small vacancy agglomerates. (2) Carbon atoms act as strong trapping sites for monovacancies. Carbon-vacancy pairs are formed at 220 K. (3) Carbon atoms are further trapped by both vacancy clusters and carbon-vacancy pairs during carbon migration at 350 K. (4) Carbon-vacancy pairs or complexes are dissociated at 490 K. This results in a second release of free monovacancies to the lattice. (5) Vacancy agglomerates anneal out around 500–600 K.

V. ESTIMATION OF VACANCY CONCENTRATIONS

In this section we reconsider the positron data for electron-irradiated samples and calculate the positron trapping rates κ_v and κ_{cl} into vacancy-type defects and vacancy clusters, respectively, following the lines pointed out in Sec. III. From the calculated values of κ_v and κ_{cl} we then estimate the defect concentrations c_v and c_{cl} by using the equations $\kappa_v=\mu_v c_v$ and $\kappa_{cl}=\mu_{cl}c_{cl}$. However, below 120 K, and in most cases also below 200 K, we have saturation trapping of positrons, wherefore the trapping-rate calculations and consequently the defect-concentration estimations are not possible at these temperature regions. For the evaluation of the specific trapping rates μ_v and μ_{cl} we consider the following cases.

(1) Comparative defect-concentration estimations were made by residual resistivity measurements. For pure iron (samples *A* and *B* in Table I) we used measurements reported[14] on samples irradiated simultaneously with our specimens. For other samples we took the irradiation-induced resistivity increase from Table I, which we scaled to the results of Leveque *et al.*[16] obtained with a similar specimen material. We used the Frenkel-pair resistivity of 30 $\mu\Omega$ cm/at.%.[8] We have further assumed that the interstitial-atom clustering does not affect the resistivity. In this case the measured resistivity values are proportional to the vacancy concentration at least up to 200-K annealing.

(2) When estimating the specific trapping rate into vacancies μ_v, we apply the results of Fig. 2 obtained in pure iron irradiated to the lower dose (sample *A*). Below 200 K single vacancies are the only type of defect detected by positrons. However, below stage I_E the vacancy concentration is so high that all positrons are trapped, making it impossible to estimate the trapping rate. Instead, between 140 and 200 K only a part of the positrons are trapped by vacancies. At this temperature range the average lifetime stays almost constant as seen in Fig. 2. When its value $\bar{\tau}\simeq 145$ psec is substituted into Eq. (7) we obtain for the trapping rate $\kappa_v=(10.5\pm 1)\times 10^9$ sec^{-1}. The observed[14] resistivity value at 160 K is $\rho(160\text{ K})=29$ nΩ cm corresponding to a Frenkel-pair concentration of 9.5 ppm. Applying now Eq. (4) we finally get a value for the specific trapping rate $\mu_v=(1.1\pm 0.2)\times 10^{15}$ sec^{-1}. This value is in excellent agreement with the one obtained by Schäfer *et al.*[31] from simultaneous resistivity and annihilation line-shape mea-

surements on iron specimens with various electron doses.

(3) Vacancy-type defects such as carbon-vacancy pairs exist between 200 and 350 K. As no information on the specific trapping rate μ_{cv} is available, we used the monovacancy value μ_v. This causes probably a slight underestimation of the pair concentration c_{cv}.

(4) Vacancy clusters are found above 200 K. No experimental data for the specific trapping rate μ_{cl} exists as a function of the cluster size. However, theoretical calculations by Nieminen and Laakkonen[40] show that μ_{cl} is proportional to the number of vacancies in the cluster in the case of small cluster radii. Denoting $\kappa_{cl}=\mu_v c_{cl}^*$, where μ_v is the specific trapping rate into monovacancies, we get a quantity c_{cl}^* giving the effective concentration of vacancies, which are bound within the vacancy agglomerates. If the average number of vacancies in a cluster is $\bar{N}$, the actual cluster concentration thus becomes

$$c_{cl}=\frac{c_{cl}^*}{\bar{N}} . \tag{12}$$

From the measured values of $\tau_2=300-400$ psec we can roughly estimate[22] that $\bar{N}\cong 5-10$.

(5) The discontinuity in Figs. 5 and 6 at 340 K is due to the temperature-dependent positron trapping rate μ_{cl} into vacancy clusters. At this temperature and above it we have increased the value for the specific trapping rate into vacancy clusters by a factor of 2.5 in evaluating c_{cl}^* to eliminate the discontinuity on the concentration scale. The specific trapping rate into the vacancy-type defects remains unchanged.

A. Electron-irradiated pure iron

Figure 11 gives the concentrations of vacancy-type defects c_v as well as those bound to vacancy clusters c_{cl}^* as a function of the isochronal annealing temperature in the pure electron-irradiated iron specimens (*A* and *B* in Table I). In the figure we have combined the results from resistivity measurements (dashed lines) with those from positron-lifetime measurements (data points).

At 77 K there are no vacancies in cluster form ($c_{cl}^*=0$) while the monovacancy concentrations are $c_v=103$ ppm and $c_v=47$ ppm for the high (6×10^{18} e^-/cm^2) and low (3×10^{18} e^-/cm^2) dose specimens, respectively. During annealing up to 140 K a sharp decrease in c_v occurs. This originates from the well-known interstitial migration

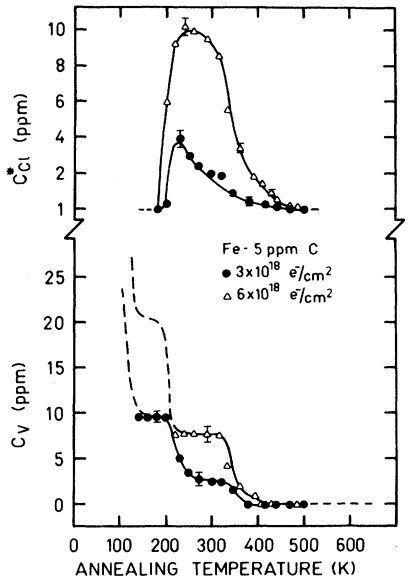

FIG. 11. Concentrations of free (below 220 K) and impurity-associated (above 220 K) monovacancies c_v, as well as the vacancy concentration c_{cl}^* bound within vacancy agglomerates as a function of the isochronal annealing temperature in electron-irradiated pure iron. The dashed lines come from resistivity measurements while the data points are constructed from the positron results in Figs. 2 and 3. The error bars are statistical resulting from standard deviations in the positron parameters.

stage I_E causing the recombination of about 80% of vacancies. In the region of stage II (140–180 K) the monovacancy concentrations level to the values $c_v\sim20$ ppm and $c_v\sim10$ ppm. This agrees well with the idea that stage II is due to a rearrangement of interstitial agglomerates, which have no effect on positron annihilation parameters.

Vacancy migration around 220 K leads to drastic changes in Fig. 11: a sharp decrease in c_v is accompanied by an appearance of vacancy clusters. From the values of c_{cl}^* and c_v we find that in the case of the lower-dose sample 28% of vacancies present just below stage III form clusters, 48% anneal out, and 24% remain in the lattice. The corresponding figures for the higher-dose specimen are 45%, 20%, and 35%. Thus monovacancies have a remarkably strong tendency to form clusters in both samples. In the higher-dose sample the cluster concentration is also higher.

From Fig. 11 we see that a part of vacancy-type defects preserve their capability of positron trapping even beyond the vacancy-migration stage III. Their residual concentrations are of the order of 7 and 2 ppm. On the basis of the previous discus-

sion on carbon-doped specimens in Sec. IV B, this can be due to vacancy capture by residual impurities in the lattice. Another possibility is vacancy clustering into dislocation loops, which are known to exhibit vacancy-type trapping properties for positrons. At 350 K, where free carbon atoms are known to migrate, c_v drops to zero. Above this temperature no positron trapping into vacancy-type defects is observed. This fact strongly indicates that the actual carbon concentration in our specimen is higher than the nominal purity $c_c < 5$ at. ppm. The carbon contamination may have occurred while manipulating the specimen. Above 400 K only vacancy clusters are detected by positrons. As can be seen from Fig. 11, the coarsening and annealing of these clusters occur in a very broad temperature range of 250–500 K, at the end of which all defects have disappeared.

B. Electron-irradiated carbon-doped iron

Figure 12 gives the concentrations c_v (below 220 K), c_{cv} (above 220 K), and c^*_{cl} for the carbon-doped iron specimens (*C* and *D* in Table I). Owing to a much higher irradiation dose compared to those in Fig. 11, the temperature region for saturation trapping of positrons extends up to 220 and 320 K for specimens containing 50 and 750 at. ppm C, respectively. Below these temperatures we have again extended the positron results with the corresponding residual resistivity curves. A special case are the results for the Fe–750 at. ppm C specimen between 220 and 320 K. We observe positron trapping at two different defect populations, carbon-vacancy pairs and vacancy clusters with the total positron trapping probability of 100%. In the limit of large trapping rates the intensities of the positron lifetimes at the defects are proportional to the corresponding trapping rates. According to Fig. 7 the intensities I_2 and I_1 are about 8 and 92%, respectively, and thus the ratio of the defect concentrations $c^*_{cl}/c_{cv} = 8/92$. We further assume that the estimated resistivity value is proportional to the total number of vacancies, i.e., to the sum $c^*_{cl} + c_{cv}$ (as in the case of interstitials, vacancy clustering does not affect the resistivity value). Combining these results we get the values for c_{cv} and c^*_{cl} between 220 and 320 K, as indicated in Fig. 12.

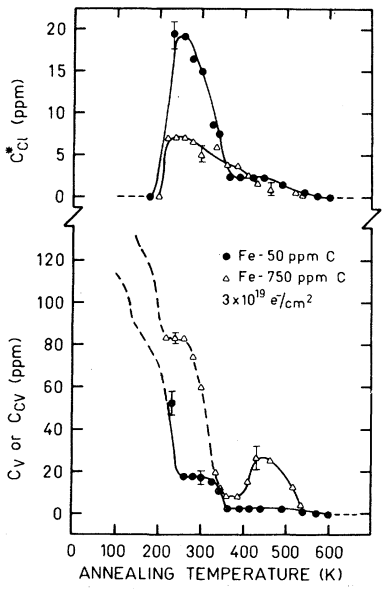

FIG. 12. Concentration of monovacancies c_v (below 220 K), carbon-vacancy pair concentration c_{cv} (above 220 K), and effective concentration c^*_{cv} of vacancies, which have been absorbed by vacancy agglomerates as a function of the isochronal annealing temperature in electron-irradiated iron-carbon samples. Dashed lines come from resistivity measurements and the data points are from the positron results in Figs. 6 and 7.

After irradiation the vacancy concentrations in the two specimens are about 550 ppm (cf. Table I). In Fig. 12, only the stage II region is indicated. At these temperatures the vacancy concentrations are about 100 ppm. In the region of stage III around 220 K, large changes in defect structure are again observed. The effective concentration of vacancies within clusters rises sharply from zero and the vacancy concentration diminishes. However, in spite of identical doses in the two specimens we see that with increasing carbon concentration the number of vacancies within the agglomerates c^*_{cl} is much smaller, while the concentration of vacancies c_{cv} remaining beyond stage III and forming pairs with carbon atoms is much higher in the Fe–750 at. ppm C specimen. Carbon atoms thus capture single vacancies, very effectively preventing their clustering. The remaining carbon-vacancy pair concentrations are about 20 and 80 ppm in the two specimens at 260 K.

Free-carbon migration at 350 K results in a sharp decrease of both c^*_{cl} and c_{cv} in Fig. 12. Carbon atoms interact with vacancy clusters and carbon-vacancy pairs, making them ineffective as positron traps. A few of both kinds of defects survive the carbon inclusion and they anneal out around 600 K. However, an increase in c_{cv} occurs in the Fe=750 at. ppm C specimen at 400 K,

where also vacancy clusters anneal out smoothly. The explanation for the increase in c_{cv} is not clear. At this temperature range carbide formation is known to occur.[13] To check the possibility of positron trapping into carbon precipitates, we also performed additional measurements after isochronal annealing of an unirradiated Fe—750 at. ppm sample which was made by an identical sample preparation technique. However, positron-lifetime measurements did not show any deviation from the free positron lifetime $\tau_f = 110$ psec during annealing treatments between 300 and 700 K. Thus positron trapping into carbon precipitates seems to be ruled out. However, it may be possible that carbon precipitates have a different structure in the irradiated sample because of the presence of irradiation-produced defects acting as nucleation sites for precipitates.

Results on defect-concentration evaluations in the Fe—50 at. ppm C samples E and F irradiated to the lower doses of 3×10^{18} and 1×10^{18} e^-/cm^2 are presented in Figs. 13 and 14, respectively. In Fig. 13, extending from 77 to 600 K, all essential features described above are visible. During stage III a small fraction of vacancies forms clusters, while the majority forms pairs with immobile carbon atoms. The carbon migration stage again results in a sharp decrease of both c^*_{cl} and c_{cv}. However, using an improved experimental setup (cf. Sec. IV C) we are now able to detect carbon-vacancy pairs ($c_{cv} \sim 4$ ppm) also above 350 K. There we can follow the annealing behavior of carbon-vacancy pairs or possibly higher-order carbon-vacancy complexes formed during carbon migration. As shown in Fig. 13 a distinct recovery stage in c_{cv} occurs around 480 K, where the pair concentration drops to zero. Also a slight increase is seen in the effective vacancy concentration within the clusters c^*_{cl}. Thus carbon-vacancy pairs or complexes are dissociated at this temperature, resulting in a release of free monovacancies bound to vacancy agglomerates as reflected through the increase in c^*_{cl}.

Figure 14 presents the estimated defect concentrations in the smaller-dose Fe—50 at. ppm C sample with the annealing temperatures shown only above room temperature. As stage III has already occurred, we observe a small concentration $c^*_{cl} \sim 0.3$ ppm of vacancies within clusters, while the carbon-vacancy pair concentration is $c_{cv} \sim 4$ ppm. Carbon migration again results in a diminishing of both kind of defects. Above 350 K we have $c_{cv} \sim 3$ ppm. During further annealing c_{cv} stays constant

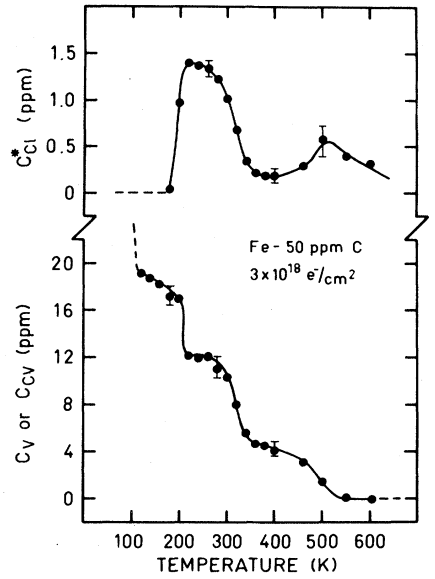

FIG. 13. The corresponding data to that in Fig. 12 for the low-dose electron-irradiated Fe—50 at. ppm C specimen in Fig. 9.

up to 460 K, and a clear recovery stage for c_{cv} is observed around 490 K. The dissociation of carbon-vacancy complexes again increases c^*_{cl} as the released vacancies are absorbed within vacancy clusters analogously with Fig. 13.

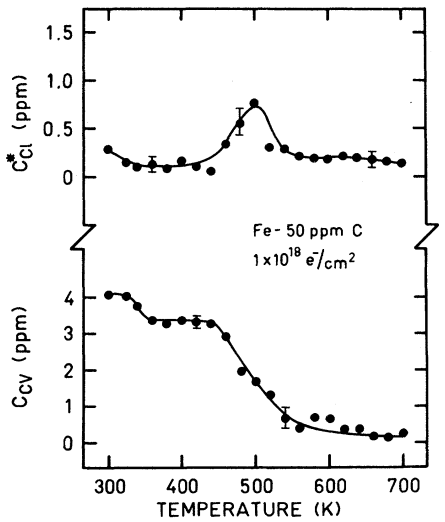

FIG. 14. Concentration of carbon-vacancy pairs c_{cv} and that of vacancies bound within vacancy clusters c^*_{cl} as a function of isochronal annealing temperature in the lowest-dose electron-irradiated Fe—50 at. ppm C sample. Only annealing temperatures above 300 K are shown. The data points are constructed from the results in Fig. 10.

VI. DISCUSSION

A. Pure iron

Our measurements reveal a drastic decrease in the vacancy concentration in iron around 220 K linked with the formation of defects having a remarkably long positron lifetime. Such a phenomenon can be unambiguously attributed to the presence of small vacancy agglomerates having three-dimensional character.[38] A significant fraction of vacancies in pure α-iron is absorbed by the growing vacancy clusters. These agglomerates have a stability limit of 500–550 K.

The most striking result of our measurements is that the free migration of monovacancies is responsible for stage III around 220 K. The experimental value,[5,6,41] for the activation energy associated with stage III is 0.55 eV. According to the present results this corresponds to the monovacancy migration energy, i.e., $E_M^{1v}=0.55$ eV. This value for the vacancy migration energy is in good agreement with the calculations of Johnson[42] and Beeler and Johnson[43] who get $E_{M,\mathrm{calc}}^{1v}=0.68$ eV. Our experiments thus give support to a value for the vacancy migration energy, which is significantly lower than the 1.28 eV deduced from higher-temperature measurements.[6]

The measured curves also give indirect information on stages I_E (120 K) and II (140–180 K). At stage I_E a strong decrease in vacancy concentration is observed, reflecting the recombinations of Frenkel pairs via migration of self-interstitial atoms. During stage II a practically constant vacancy concentration is observed. This is compatible with the idea that some rearrangements of interstitial-atom clusters take place within this temperature range.

B. Carbon-doped iron

All experimental results of the present work on the role of carbon atoms in the annealing kinetics of point defects demonstrate the strength of the carbon-vacancy interaction in α-iron. During the migration of monovacancies at 220 K, carbon atoms decrease the fraction of clustered vacancies and increase the fraction of residual vacancies remaining in the lattice. The mobile vacancies react strongly with immobile carbon atoms, and stable carbon-vacancy pairs are formed. A striking feature is that positrons are still able to get localized at the site of carbon-vacancy pairs.

An opposite phenomenon has been shown to occur in copper, where positrons are insensitive to vacancies at the presence of a hydrogen atom in a vacant lattice site.[44] The positron lifetime $\tau_{cv}=160$ psec is only slightly lower than the one for vacancies $\tau_v=175$ psec. On the basis of these observations we argue that the structure of the pair must have a highly asymmetric character, i.e., the pair does not recombine into a substitutional carbon atom. Such an idea of a carbon atom bound to the boundary region of a monovacancy is consistent with the calculations of Johnson and Damask.[45] They reported the carbon position at 0.73 half-lattice constants from the center of the vacancy along ⟨100⟩ direction, i.e., not far from the neighboring octahedral position.

Our results show that the migration sequence of the constituents of the carbon-vacancy pair is reversed from what has been generally assumed: it is a stable carbon atom that captures a migrating vacancy. One of the consequences of this reversed situation is the fact that defect reactions occurring during carbon migration at 350 K have been totally misinterpreted.[10,17–19] For instance, the energy which is released during the stage and for which the value of 0.41 eV was obtained calorimetrically by Arndt and Damask,[17] has been considered as the binding energy between the vacancy and the associated carbon atom. From our point of view, this energy corresponds to the binding of additional carbon atoms to the pairs and vacancy agglomerates present in the lattice just below 350 K. Takeyama and Takahashi[18,19] used room-temperature high-voltage electron microscope (HVEM) irradiation to produce monovacancies, which were expected to react with carbon atoms and cause thus the absence of carbon precipitation during further annealing. Again their basic assumption must be modified: carbon-vacancy pairs are formed in abundance already during irradiation. On the other hand, their conclusion on the presence of carbon-vacancy pairs above room temperature, which hinders carbon precipitation, is correct. Their results also give important information on the stability limit of carbon-vacancy pairs: precipitation is again observed after 510 K annealing. The authors attributed this temperature to the dissociation of the pairs.

Our results on the stability of carbon-vacancy pairs (Figs. 13 and 14) are in agreement with those of Takeyama and Takahashi.[18,19] We observe the disappearance of the pairs at 490 K. This roughly corresponds to the dissociation energy of 1.4 eV.

Taking this value to be equal to the sum of the binding energy and the migration energy of the faster-moving constituent (the vacancy with $E_M^{1v}=0.55$ eV), we obtain an estimate for the carbon-vacancy binding energy $E_B^{cv}\sim 0.85$ eV. This very high value indicates a high stability for the pair. The energy is also significantly higher than the value 0.41 eV (Ref. 17) mentioned previously.

Some indirect conclusions can be made from our results in pure and carbon-doped iron irradiated to a dose of 3×10^{18} e^-/cm^2 (cf. Figs. 11 and 13). After stage I_E a much higher vacancy concentration remains in the carbon-doped specimen compared to the pure iron. This reflects the interaction of carbon with iron interstitial atoms. Such an interaction, attributed to trapping of interstitial atoms by carbon impurities, is observed in various experiments.[14,16,41,46] Additional stages are also observed in carbon-doped iron at 160–180 K (Refs. 16 and 41) associated with decomposition of interstitial-carbon complexes. These ideas are also compatible with our results. In carbon-doped iron the vacancy concentration decreases at this temperature range (Fig. 13), while it is virtually constant in pure iron (Fig. 11). Thus our results agree with the idea of dissociation of carbon-self-interstitial pairs around 170 K. This corresponds to the binding energy of the pairs $E_B^{ci}\sim 0.1$ eV.[41]

As mentioned previously, the well-known stage for carbon migration at 350 K is governed by a strong interaction of carbon with the remaining point defects, i.e., carbon-vacancy pairs and vacancy clusters. This decoration of carbon-vacancy pairs with additional carbon atoms can be easily visualized. There are six equivalent positions for the carbon around the vacancy; occupation of these positions decreases the free space for positron localization, thus preventing trapping. Carbon migrates also to the vacancy agglomerates, which is seen as a decrease of their effective concentration. Such a "nullification" of positron trapping at 350 K has been observed earlier by Snead *et al.*,[47] although their interpretation was based on immobile vacancies at room temperature.

C. Controversial aspects on vacancy migration

Our positron-lifetime results have revealed free vacancy migration in α-iron in stage III at 220 K. We consider this result conclusive, leaving no space for other interpretations. The temperature range of vacancy migration is surprisingly low compared to, e.g., other transition metals. However, as Schultz[48] has pointed out, the vacancy migration energy must not be scaled to the melting temperature T_m, but rather to the values of the elastic constants which are low for the group-V transition metals and for α-iron.

There exist a lot of experiments which support the low migration energy of vacancies. Detailed residual-resistivity measurements on electron-irradiated iron-carbon samples[41] have lead to conclusions with vacancies mobile at 220 K. Similar ideas have been presented also on the basis of perturbed angular-correlation measurements of ^{111}In in iron.[49] Positron results in neutron-irradiated iron (see the second part of this paper and references therein) show a downward shift in the migration temperature of vacancies due to the higher local vacancy concentration within the collision cascades. The present situation has been recently discussed by Takaki *et al.*[41] and de Schepper *et al.*[50]

Yet, as discussed in Sec. I, a considerable group of experimental results seemed to point strongly towards vacancy migration at 520 K. In the following, some reasons for this long standing controversy will be considered. Our results point out the main clue to this discrepancy: the enormous sensitivity of point defects to very small quantities of interstitial carbon impurities. These two defects couple with each other very effectively and therefore vacancy properties are fully masked by those of higher-order complexes. On the other hand, residual carbon concentration is present in most experimental conditions in amounts sufficient to drastically change the kinetics of point defects. A good example is shown in Fig. 13, where the annealing stages both at 220 and 500 K are associated with monovacancy motion in the lattice, resulting in a decrease of the vacancy concentration and an increase in the number of clustered vacancies. In the following we make some suggestions concerning the reasons for the controversial results in some experiments mentioned in Sec. I.

Kiritani *et al.*[9] deduced vacancy mobility by observing a threshold temperature and kinetics of the shrinkage and growth of interstitial loops, obtaining a vacancy migration energy of 1.25–1.5 eV. However, the high tendency for vacancies to agglomerate as well as to form pairs with residual impurities has not been taken into account. Recent experiments of Verdone *et al.*[51] using very high-purity iron result in a vacancy migration energy around 0.6 eV. Kiritani *et al.*[52] obtain a value of

$E_M^{1v}=0.72$ eV with a specimen of $RRR_H=3500$. Fujita *et al.*[53] deduce a vacancy migration energy of $E_m^{1v}=0.57$ eV for pure Fe with $RRR_H=8800$. Both Kiritani *et al.* and Fujita *et al.* also obtain $E_M^{1v}\sim 1.2$ eV in the case of a lower-purity sample with $RRR_H \lesssim 1500$.

A magnetic after-effect band arising above 300 K has been attributed to the formation of carbon-vacancy pairs via migration of carbon atoms[10] into stable vacancies at room temperature. However, another band arises already at 220 K,[46,54] which can also be attributed to the pairs formed via vacancy migration. The successive band arising above 300 K is then due to "decorated" carbon-vacancy complexes mentioned previously. The magnetic after-effect findings of Vigier[55] give further support to our results and conclusions. The impurity-dependent magnetic after-effect zones generated successively after stage I_E in pure and impurity-doped iron disappear after 240 K annealing regardless of the type and concentration of impurities present. Since these bands are generally interpreted to be due to impurity-self-interstitial complexes having varying binding energies, a natural explanation of this phenomenon is the disappearance of these defects via recombinations with their migrating antidefects, i.e., the vacancies. In doped iron the magnetic after-effect zones due to substitutional impurity-monovacancy complexes are fully developed after room-temperature irradiation,[56] because vacancies have migrated into the impurities in the course of the irradiation. Also, the internal friction measurements[14] can be analogously explained using both models for vacancy migration.

Kuramoto *et al.*[11] have studied the temperature dependence of void swelling in α-iron. They assumed the threshold temperature of about 600 K to be governed by the mobility of monovacancies. Again, the formation of very stable vacancy agglomerates and vacancy-impurity pairs dissociating at 500–600 K can account for the absence of void swelling at moderate temperatures. In fact, Little[57] has suggested the carbon-vacancy pair formation to be responsible for the very low peak-swelling value for α-iron. The influence of small amounts of carbon has indeed been shown to effect drastically the void-swelling behavior.[58]

Studies of radiation doping by Takamura[12] can be used for the deduction of vacancy properties. In radiation-doping studies an irradiated specimen is first annealed at an intermediate temperature, whereafter a second irradiation is performed. An enhanced recovery stage I_E is observed only in case the intermediate annealing temperature is below the vacancy migration threshold. With this method Takamura obtained 410 K for the temperature of vacancy migration. Our results give again reason to modify this picture. If a considerable fraction of vacancies is bound to higher-order complexes, the temperature obtained by Takamura corresponds to the stability limit of the complexes instead of that for monovacancies. This is particularly the case here, because Takamura used neutron irradiation, where a far larger fraction of vacancies form clusters (see the second part of the present paper).

The observation of quenched-in vacancies in iron has proven to be very difficult.[13] Most experiments are involved with phenomena above room temperature, where our results do not allow the presence of free vacancies. Recent experiments[41] seem to confirm that no vacancy stage can be found in pure iron, while they are abundantly present in carbon-doped specimens after quenching at room temperature. This is exactly what is to be expected on the basis of our results.

Finally, a strong argument for the vacancy migration above room temperature has been provided by the combined positron annihilation and self-diffusion measurements[15] which give the value of 1.28 eV for the monovacancy migration energy.[6] However, there exist some doubts against this result. The self-diffusion measurements are extremely sophisticated, involving, e.g., diffusion times of the order of several days. Furthermore, the resulting diffusion coefficient does not follow a simple Arrhenius law because of complications by ferromagnetic transition. Carbon and other impurities are also expected to have a large influence on the diffusion behavior, as discovered by Irmer *et al.*[59] Furthermore, preliminary calculations carried out by de Schepper *et al.*[60] seem to point towards a strong influence of carbon on the measured value for the vacancy formation energy. Thus the assumption[15] that the diffusion mechanism is governed by monovacancy processes may not be entirely justified.

VII. CONCLUSIONS

We find the following conclusions.

(1) In electron-irradiated α-iron our positron-lifetime measurements show free monovacancy mi-

gration at stage III around 220 K.

(2) At stage III monovacancies have a remarkably strong tendency to form small, three-dimensional vacancy agglomerates. These anneal out around 500–600 K.

(3) In carbon-doped specimens a competing reaction at stage III is the formation of a bound carbon-vacancy pair. This defect is strongly asymmetric, as shown by the strong positron trapping ability of the pair. The pair dissociates at 490 K.

(4) Unpaired carbon atoms migrating at 350 K interact further with defect complexes, e.g., carbon-vacancy pairs and vacancy agglomerates. This leads to a decrease of positron trapping into both type of defects.

ACKNOWLEDGMENTS

We are indebted to Section des Accélérateurs of Centre d'Etudes Nucléaires, Grenoble for low-temperature electron irradiations. The authors thank K. Rytsölä for his efforts in developing the positron-lifetime equipment. The contributions of T. Judin, L. Määttänen, and P. Saariaho in the positron experiments are gratefully acknowledged. The assistance of R. Komu, T. Poikolainen, and R. Talja from the University of Jyväskylä, Finland in preparing the proton-irradiated positron sources deserves our gratitude. We wish to thank H. Schultz, F. Pleiter, and L. Stals for communication of their results prior to publication.

[1]J. Nihoul, in *Vacancies and Interstitials in Metals,* edited by A. Seeger, D. Schumacher, W. Schilling, and J. Diehl (North-Holland, Amsterdam, 1970), p. 839.

[2]M. Weller and J. Diehl, in *Internal Friction and Ultrasonic Attenuation in Solids,* edited by R. R. Hasiguti and N. Mikoshiba (University of Tokyo Press, Tokyo, 1977), p. 425.

[3]P. Moser, in *Internal Friction and Ultrasonic Attenuation in Solids,* edited by R. R. Hasiguti and N. Mikoshiba (University of Tokyo Press, Tokyo, 1977), p. 63.

[4]H. Kimura, in *Progress in the Study of Point Defects,* edited by M. Doyama and S. Yoshida (University of Tokyo Press, Tokyo, 1977), p. 119.

[5]L. J. Cuddy, Acta Metall. 16, 23 (1968).

[6]W. Decker, J. Diehl, A. Dunlop, W. Frank, H. Kronmüller, W. Mensch, H. E. Schäfer, B. Schwendemann, A. Seeger, H. P. Stark, F. Walz, and M. Weller, Phys. Status Solidi A 52, 239 (1979).

[7]H. Wever and W. Seith, Phys. Status Solidi A 28, 187 (1975).

[8]F. Maury, M. Biget, P. Vajda, A. Lucasson, and P. Lucasson, Phys. Rev. B 14, 5303 (1976).

[9]M. Kiritani, H. Takata, K. Moriyama, and F. Fujita, Philos. Mag. A 40, 779 (1979).

[10]F. Walz, H. J. Blythe, and H. Kronmüller, Phys. Status Solidi A 61, 607 (1980).

[11]E. Kuramoto, K. Futajami, and K. Kitajima, in *Proceedings of the 5th International Conference on High Voltage Electron Microscopy,* (Japan Society of Electron Microscopy, Tokyo, 1978), p. 589.

[12]S. Takamura, Radiat. Eff. Lett. 43, 69 (1979).

[13]S. Takaki, and H. Kimura, Scr. Metall. 10, 1095 (1976).

[14]M. Weller, J. Diehl, P. Moser, M. Dubus, and P. Hivert, in *Internal Friction and Ultrasonic Attenuation in Solids,* edited by C. C. Smith (Pergamon, New York, 1980), p. 181.

[15]J. Diehl, U. Merbold, and M. Weller, Scr. Metall. 11, 811 (1977).

[16]J. L. Leveque, T. Anagnostopoulos, H. Bilger, and P. Moser, Phys. Status Solidi 31, K47 (1969).

[17]See series of papers: H. Wagenblast and A. C. Damask, J. Phys. Chem. Solids 23, 221 (1962); F. E. Fujita and A. C. Damask, Acta Metall. 12, 331 (1964); R. A. Arndt and A. C. Damask, *ibid.* 12, 341 (1964); H. Wagenblast, F. E. Fujita, and A. C. Damask, *ibid.* 12, 347 (1964).

[18]T. Takeyama and H. Takahashi, J. Phys. Soc. Jpn. 35, 939 (1973).

[19]T. Takeyama and H. Takahashi, in *Fundamental Aspects of Radiation Damage in Metals,* edited by M. T. Robinson and F. W. Young, Jr. (ERDA, Oak Ridge, 1976), p. 1100.

[20]*Positrons in Solids,* Vol. 12 of *Topics in Current Physics,* edited by P. Hautojärvi (Springer, Heidelberg, 1979).

[21]R. W. Siegel, Ann. Rev. Mater. Sci. 10, 393 (1980).

[22]P. Hautojärvi, J. Heiniö, M. Manninen, and R. Nieminen, Philos. Mag. 35, 973 (1977).

[23]P. Hautojärvi, T. Judin, A. Vehanen, J. Yli-Kauppila, J. Johansson, J. Verdone, and P. Moser, Solid State Commun. 29, 855 (1979).

[24]P. Hautojärvi, J. Johansson, T. Judin, P. Moser, M. Puska, A. Vehanen, and J. Yli-Kauppila, in *Proceedings of the 5th International Conference on Positron Annihilation,* edited by R. R. Hasiguti and K. Fujiwara (Japan Institute of Metals, Sendai, 1979), p. 737.

[25]P. Hautojärvi, J. Johansson, A. Vehanen, J. Yli-Kauppila, and P. Moser, Phys. Rev. Lett. 44, 1326 (1980).

[26]P. Hautojärvi, J. Johansson, L. Pöllänen, A. Vehanen, J. Yli-Kauppila, and P. Moser, in *Proceedings of the EPS Conference on Nuclear Physics Methods in Materials Science,* edited by K. Bethge, H. Baumann, H. Jex, and F. Rauch (Vieweg, Braunschweig, 1980), p. 454.
[27]F. Vanoni, thesis, University of Grenoble, 1973 (unpublished).
[28]K. Hinode, S. Tanigawa, M. Doyama, and N. Shiotani, Appl. Phys. 20, 185 (1979).
[29]A. Vehanen (unpublished).
[30]See, e.g., R. West, p. 90 in Ref. 20.
[31]H.-E Schäfer, P. Valenta, and K. Maier, in *Proceedings of the 5th International Conference on Positron Annihilation,* edited by R. R. Hasiguti and K. Fujiwara (Japan Institute of Metals, Sendai, 1979), p. 509.
[32]See, e.g., R. M. Nieminen, J. Laakkonen, P. Hautojärvi, and A. Vehanen, Phys. Rev. B 19, 1397 (1979) and references therein.
[33]S. Mantl and W. Triftshäuser, Phys. Rev. B 17, 1645 (1978).
[34]K. Hinode, S. Tanigawa, and M. Doyama, J. Nucl. Mater. 69&70, 678 (1978).
[35]M. Eldrup, O. E. Mogensen, and J. H. Evans, J. Phys. F 6, 499 (1976).
[36]H.-E. Schäfer, P. Valenta, B. Saile, and K. Maier, in *Proceedings of the 5th International Conference on Positron Annihilation,* edited by R. R. Hasiguti and K. Fujiwara (Japan Institute of Metals, Sendai, 1979), p. 747.
[37]W. Frank, A. Seeger, and M. Weller, Radiat. Eff. 55, 111 (1981).
[38]P. Hautojärvi and Vehanen, Radiat. Eff. Lett. 58, 77 (1981).
[39]P. Hautojärvi, A. Vehanen, and V. S. Mikhalenkov, Appl. Phys. 11, 191 (1976).
[40]R. M. Nieminen and J. Laakkonen, Appl. Phys. 20, 181 (1979).
[41]S. Takaki, J. Fuss, H. Kugler, U. Dedek, and H. Schultz, Radiat. Eff. (in press).
[42]R. A. Johnson, Phys. Rev. 134, A1329 (1964).
[43]J. R. Beeler, Jr. and R. A. Johnson, Phys. Rev. 156, 677 (1967).
[44]B. Lengeler, S. Mantl, and W. Triftshäuser, J. Phys. F 8, 1691 (1978).
[45]R. A. Johnson and A. C. Damask, Acta Metall. 12, 443 (1964).
[46]J. L. Leveque, T. Anagnostopoulos, H. Bilger, and P. Moser, Phys. Status Solidi 29, K179 (1968).
[47]C. L. Snead, Jr., A. N. Goland, J. H. Kusmiss, H. C. Huang, and R. Meade, Phys. Rev. B 3, 275 (1971).
[48]H. Schultz, Scr. Metall. 8, 721 (1974).
[49]F. Pleiter, C. Hohenemser, and A. R. Arends, Hyperfine Interact. 10, 691 (1981).
[50]L. De Schepper, J. Cornelis, G. Knuyt, J. Nihoul, and L. Stals, Phys. Status Solidi A 61, 341 (1980).
[51]J. Verdone, A. Bourret, and P. Moser, Radiat. Eff. (in press).
[52]Private communication.
[53]Private communication.
[54]J. Verdone, P. Moser, W. Chambron, J. Johansson, P. Hautojärvi, and A. Vehanen, J. Magn. Magn. Mater. 19, 296 (1980).
[55]P. Vigier, thesis, University of Grenoble, 1968 (unpublished).
[56]P. Moser, Mem. Sci. Rev. Metall. 63, 431 (1966).
[57]E. A. Little, J. Nucl. Mater. 87, 11 (1979).
[58]L. De Schepper, G. Knuyt, and L. Stals, in *Nuclear Physics Methods in Materials Research,* edited by K. Bethge *et al.* (Vieweg, Braunschweig, 1980), p. 468.
[59]V. Irmer and M. Feller-Kniepmeier, Philos. Mag. 25, 1345 (1972).
[60]L. De Schepper, G. Knuyt, and L. M. Stals, Phys. Status Solidi A 67, 153 (1981).